

Spatial-temporal assessment of water and sediment connectivity through a modified connectivity index in a subtropical mountainous catchment

Franciele Zanandrea ^{*}, Gean Paulo Michel, Masato Kobiyama, Guilherme Censi,
Bruno Henrique Abatti

Instituto de Pesquisas Hidráulicas (IPH), Universidade Federal do Rio Grande do Sul, Av. Bento Gonçalves 9500, 91509-900 Porto Alegre, RS, Brazil

ARTICLE INFO

Keywords:
Functional connectivity
Structural connectivity
Precipitation
Hydrogeomorphology

ABSTRACT

The concept of connectivity aims to understand the hydrosedimentological (water and sediments) processes that occur in the catchment and influence the water and sediment transfer at different spatial-temporal scales. Connectivity is often assessed through connectivity indexes, commonly considering only structural features of the landscape. The present study proposes the insertion of the precipitation and surface runoff characteristics as functional components to the connectivity index (*IC*). Its main goal is to evaluate the space-time variation of water and sediment connectivity in a subtropical catchment. To achieve this goal, two parameters, extracted from precipitation data, were inserted in the *IC* and resulted in the hydrosedimentological connectivity index (*IHC*), which concerns the runoff generation and the characteristics of the antecedent precipitation event. The *IHC* was tested on a catchment scale for 7 individual precipitation events. For each event, the index provided values and maps that reflected the dynamic processes of the catchment, regarding the functional and structural components of connectivity. The performance analysis of the index was qualitative, and it was carried out by means of a visual interpretation using field data on processes and sediment paths. The *IHC* map was coherent with the field data and it showed a satisfactory representation of the sediment transfer patterns. It was observed that the debris flow scars corresponded to the flow paths with higher *IHC* values and the deposition areas with the lower *IHC* values. In addition, the *IHC* values showed a positive correlation with the catchment flow values. Statistical analysis indicated a correlation between the mean *IHC* and the total runoff volume (+0.69) as well as between the mean *IHC* and the peak flow (+0.63). The *IHC* was able to estimate the space-time variation of water and sediment connectivity in a catchment, identifying locations of sediment transfer and deposition for precipitation events with different magnitudes. The modified method was able to bring advances to connectivity representation, however, it presented some limitations, such as the incapability to represent the sediment exhaustion in the catchment. Even so, the *IHC* allows its application in areas with little data and it can be a useful tool in identifying relevant sites on watershed management.

1. Introduction

Connectivity is an important concept to better understand processes occurring at a catchment level that impact the water, the sediment dynamics and other systems (e.g., biological activities) at different spatial-temporal scales (Michaelides and Chappell, 2009). The definition of sediment connectivity is presented by Bracken et al. (2015) as the physical transfer of sediments from a source through the catchment, controlled by the way in which landscape compartments are linked. In a natural setting with no significant interference of humans, different

vectors such as wind, gravity, water, and animals can be responsible for this transfer (Peters et al., 2008; Bracken et al. 2015). In places with well-distributed precipitation throughout the year (e.g., tropical and subtropical regions), such transfer is caused mainly by water which displaces material in different time-space variations.

Sediment connectivity analysis have received more attention (Bracken et al., 2015) by often using indexes for connectivity evaluation. Borselli et al. (2008) proposed a sediment connectivity index (*IC*) based on a geomorphological approach, in which hydrological processes are not explicitly considered. Instead, the *IC* is based on the physical

* Corresponding author.

E-mail addresses: franciele.zanan@gmail.com (F. Zanandrea), gean.michel@ufrgs.br (G.P. Michel), masato.kobiyama@ufrgs.br (M. Kobiyama), guilherme.censi@hotmail.com (G. Censi), bruno.abatti@gmail.com (B.H. Abatti).

characteristics of the upstream area and downstream path in relation to a determined point, considering the topographic attributes of the landscape and the sediment impedance. The *IC* represents the possibility of sediment from a certain location to reach a sink or a drainage network, which is calculated for each point of the terrain.

The connection between elements of the landscape originated from surface and subsurface flows is represented by the functional component of connectivity (Turnbull et al., 2008; Duvert et al., 2011; Wainwright et al., 2011). The other component of connectivity refers to the spatial patterns of the landscape, defined by the same authors as a structural element. It depends on the path (continuity), the length of the slope, and the impedance (resistance) to the flow (Bracken et al., 2013).

According to Heckmann et al. (2018), connectivity becomes an emergent property of the system state, reflecting the continuity and strength of the water flow and sediment paths over a given time interval. In such a way, the structural characteristics, linked to the landscape geomorphology, provide spatial dimensions to the connectivity, while the functional aspects, linked to the hydrological properties, evaluate a time-scale variation. Thus, connectivity is modified over time on a specific space-time scale (Nunes et al., 2018).

The temporal variability of the connectivity is the key to understand the short-term sediment dynamics, especially in catchments that experience a strong seasonality in precipitation rates (Mishra et al., 2019). Climate regimes are typically controlled by altitude in tropical mountains regions (Leigh, 1975). According to Wohl (2010), mountainous morphologies are controlled by tectonics, lithology, climate, and vegetation, which in turn control the water and sediments dynamics. Higher regions usually experience lower temperatures and higher precipitation rates, especially during the summer season. These climatic factors affect the hydrosedimentological dynamics of the catchment.

In mountainous regions, landslides and debris flows are also important sources of sediment (Ward, 1997) and they alter hydrosedimentological processes in the catchment. Furthermore, landslides can impede the sediment flux which abruptly changes the connectivity according to Korup et al. (2004). Not all materials moved by landslides are able to reach the channel. When there is no connection between source and target, the moved material may be (re)deposited on its path. Jones and Preston (2012) mentioned that disconnected sediment is stored temporarily on the paths, but it will eventually reach the target by subsequent precipitation events. This condition may modify the frequency and magnitude of sediment yield events (Hicks et al., 2000).

There are significant differences in the sediment connectivity of precipitation events with different magnitudes. Functional connectivity depends on the characteristics of precipitation and antecedent conditions, such as soil moisture (Turnbull and Wainwright, 2019) and the amount of available sediment, which varies over space and time. Several studies used the soil water content to evaluate connectivity (Kalantari et al., 2019; Turnbull and Wainwright, 2019), soil permeability (López-Vicente and Ben-Salem, 2019; Zingaro et al., 2019) and saturated hydraulic conductivity (López-Vicente et al., 2013). By contrast, other studies assessed hydrological modeling (Mahoney et al., 2018) and soil erosion modeling (Zhao et al., 2020) with sediment connectivity.

Some studies evaluated the sediment connectivity considering the temporal variation (López-Vicente and Ben-Salem, 2019; Mishra et al., 2019). Mishra et al. (2019) assessed sediment connectivity at a monthly scale, analyzing the stream power of the main river and its tributaries together with the *IC* for the study catchment. However, the temporal variation in the sediment availability was not considered, neither the variations in the magnitude of events. López-Vicente and Ben-Salem (2019) considered an aggregated weighting factor within the *IC*, in addition to soil permeability and the rainfall erosivity factor, which influences the sediment availability. To account for this, the mean values of monthly rainfall erosivity were used.

Based on the above, connectivity plays a significant role in the characterization of structural properties of the landscape. When combined with forcing processes (e.g., rainfall-runoff), it can become a

useful tool for landscape management (Crema and Cavalli, 2018). Kalantari et al. (2017) evaluated connectivity by considering the runoff calculated with the Soil Conservation Service (SCS), Curve Number (CN) method (SCS, 1972), as a weighting factor (*W*) within the *IC*. Other studies modified the *IC* by adding different factors to assess potential availability of detachable sediment in *W*, such as the development and persistence of the drainage network (Gay et al., 2016), rainfall erosivity (Chartin et al., 2017; de Walque et al., 2017) and soil erodibility (de Walque et al., 2017).

The characterization of hydrologically-driven transfer processes still needs many advances to better understand the diffusiveness arising from land use activities (Lane et al., 2009). Di Stefano and Ferro (2018) observed that functional connectivity depends on the magnitude of erosion events which are tightly related to runoff generation. Therefore, the integration between runoff generation information and the connectivity index can be a useful way for further understanding of the sediment dynamics in a catchment.

Precipitation is the main driving force for surface and subsurface runoff generations, which are responsible for establishing the connection between the compartments of the landscape (Crema and Cavalli, 2018; Turnbull and Wainwright, 2019). The results obtained by Baartman et al. (2020) demonstrated that the precipitation amount is the main factor in determining the relative export of sediment and the connected areas of runoff and sediment, indicating that the functional aspects of connectivity were more important than the structural ones. Thus, the authors concluded that indexes that incorporate functional connectivity to structural ones can be more adequate, although they are less common than structural connectivity indexes and more complex to be calculated. The use of structural connectivity alone may not be sufficient to represent the connectivity of water and sediment in the catchment (Di Stefano and Ferro, 2018; Baartman et al., 2020).

Having assumed these evidences, the main goal of this study was to modify the connectivity formulation of sediment and water proposed by Borselli et al. (2008), by integrating it into the original formulation precipitation-derived variables as representative of the functional component. Here, this new index is called hydrosedimentological connectivity index (*IHC*). The index is based on the concept of sediment transport capacity and does not consider the sediment exhaustion in the catchment, which is a limitation for the methodology. In order to demonstrate its use for assessment of the spatial-temporal variation of water and sediment connectivity, the present study applied the *IHC* to a subtropical catchment in the face of different precipitation events.

2. Materials and methods

2.1. Study area

The Mascarada River catchment (Fig. 1), located in the State of Rio Grande do Sul, Brazil, is a part of Serra Geral geological formation. This catchment has an altimetric amplitude of 925 m and it contains a mountainous region with slopes varying from 18° to 85°. The catchment is approximately 33 km long and it has a contributing area of 320 km². The land uses in the catchment are native tropical forests and reforested areas (70%), agriculture (10%), pasture (8%), and urban area (1%) (Zanandrea et al., 2020). The area is characterized by shallow soils (from 0 to 2 m in depth), a significant presence of organic matter, a high clay content, and a low bulk density (Dümg et al., 2008).

The climate in the catchment is subtropical. The precipitation regime is temporally well distributed and it has an expressive thermal amplitude throughout the year. The annual precipitation varies from 1600 mm to 2000 mm. Precipitation of high intensity occurs during the summer season whereas the winter's precipitation regime is milder. Precipitation is notably regulated by orographic phenomena, in which the relief causes intense and locally-concentrated precipitation events (Wollmann and Galvani, 2012).

An extreme precipitation event occurred in Mascarada River

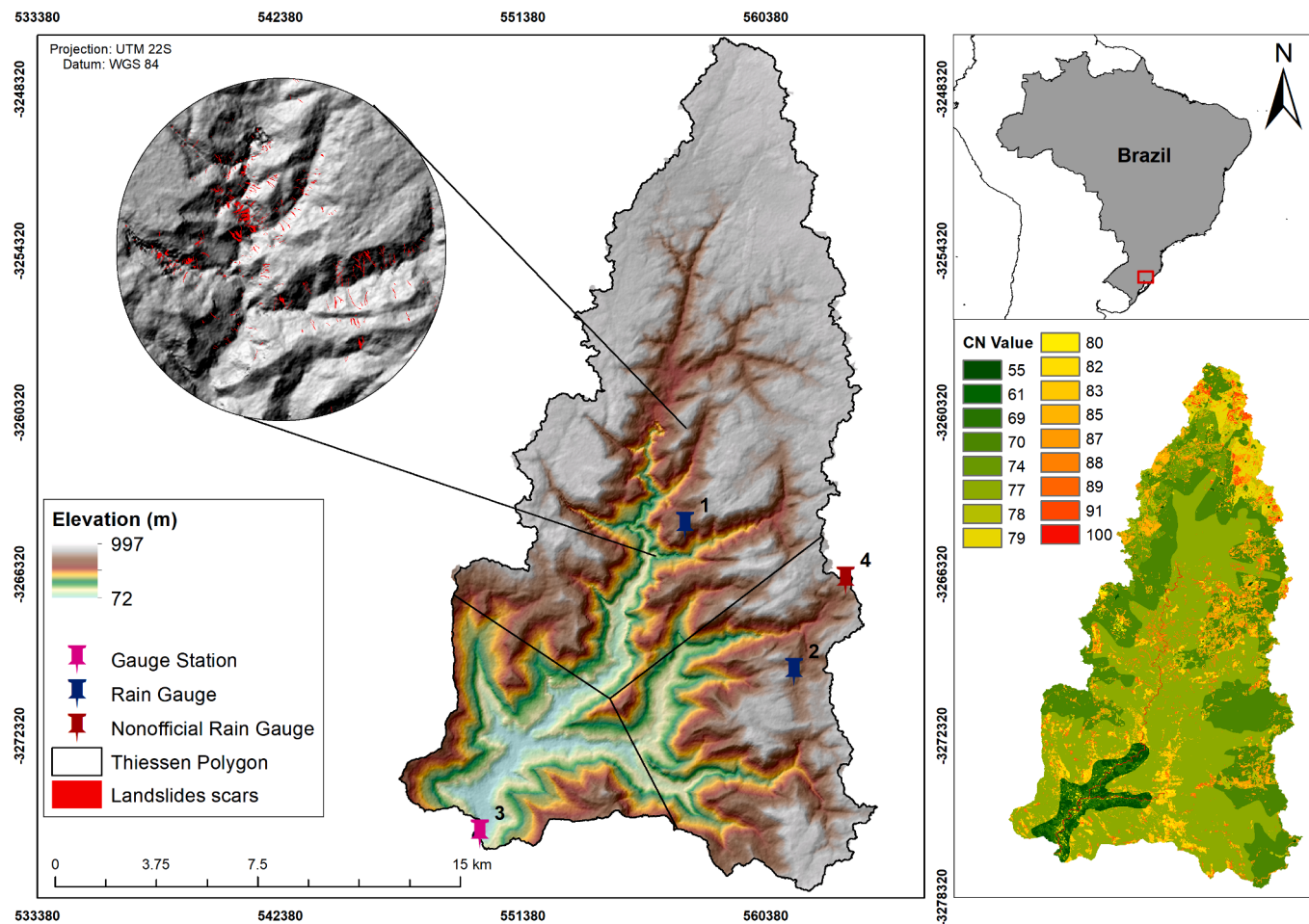


Fig. 1. Location map of the Mascarada River catchment, monitoring stations and a Curve Number (CN) map. Rolante municipality city center is located approximately 7 km downstream from the Mascarada catchment outlet.

catchment on January 5, 2017. Unofficial records of this precipitation reported values of 270 mm in 2 to 3 h, measured through rudimentary rain gauges by local farmers. This event triggered at least 420 shallow landslides and caused a flashflood in Rolante municipality. The landslides occurred on hillslopes covered by natural forest and reforested. The flood was caused by the failure of a natural dam formed by landslides during the event. Thus, this event caused a strong disturbance in the Mascarada River catchment, both in terms of sediment yield and river morphology (Zanandrea et al., 2020).

2.2. Index of sediment connectivity

This study proposes a modification of the *IC* developed by Borselli et al. (2008) considering the suggestions already incorporated by Cavalli et al. (2013). These suggestions are related to the flow accumulation algorithm and maximum slope threshold. Borselli et al. (2008), by their turn, proposed an *IC* based on topographic and land use information. This index determines, at a pixel scale, the degree of connectivity for a given point. The *IC* incorporates the characteristics of the contribution area (upstream component - D_{up}), and the characteristics of the flow path to be performed by the sediment to the point of interest (downstream component - D_{dn}). The *IC* values are presented in an interval of $[-\infty, +\infty]$ and they are calculated by the following equation:

$$IC = \log_{10} \left(\frac{D_{up}}{D_{dn}} \right) = \log_{10} \left(\frac{\overline{W} \overline{S} \sqrt{A}}{\sum_i \frac{d_i}{W_i S_i}} \right) \quad (1)$$

where W is the impedance factor; S is the slope (m/m); A is the contribution area (m^2); d is the length of the flow path of each pixel (m), *IC* is the connectivity of sediment (dimensionless).

The impedance factor represents the resistance that the land surface imposes to water and sediment flow. Because of this, the determination of this factor is dependent on the characteristics of the study area. The original *IC* uses the USLE/RUSLE factor *C*, proposed by Wischmeier and Smith (1978) and Renard et al. (1997), as the impedance factor. Cavalli et al. (2013) adapted the impedance factor to an exclusively geomorphological approach, using the residual topography (*RI*) and optimizing the *IC* application in mountainous regions, where impedance conditions are better represented by the surface roughness. Persichillo et al. (2018) sought to understand the variation in sediment connectivity as a result of land use changes, by which the Manning coefficient (*n*) was used to represent the impedance factor.

Zanandrea et al. (2020) proposed the Relative Smoothness (*RS*), which is an impedance factor based on Manning's coefficient that preserves the non-dimensionality of the index:

$$RS = \frac{n_{min}}{n} \quad (2)$$

where n_{min} is the minimum tabulated value; and n is the local Manning coefficient.

The value adopted for n_{min} in Zanandrea et al. (2020) was 0.01 which can be seen in Chow (1959). The use of *RS* proved to be advantageous in regions covered by dense forests, like the Mascarada catchment. Therefore, the same values of *RS* were used in this study for the *W* factor to estimate *IHC*.

2.3. Framework and formulation of the modified index

The proposed modification of the index is based on insertion of variables (precipitation index for sediments – Ips and surface runoff – Q_{runoff}) related to functional connectivity into the IC , considering the role of water in the sediment connectivity. Functional connectivity is related to the precipitation characteristics, the antecedent conditions (Turnbull and Wainwright, 2019) as well as the flow continuity/discontinuity through a catchment, which brings a temporal feature to connectivity. The hydrosedimentological connectivity index (IHC) is proposed in this paper to assess the spatial-temporal variation of water and sediment connectivity at the event scale. The index considers the magnitude of current and antecedent precipitation events:

$$IHC = \log_{10} \left(\frac{\overline{RS} \bar{S} Ips \sum Q_{runoff}}{\sum_i \frac{d_i}{RS_i S_i}} \right) \quad (3)$$

where Ips is the precipitation index for sediments (dimensionless), Q_{runoff} is the accumulated surface runoff (m) from the upstream drainage area of the calculated pixel, which is dependent on the pixel size.

The runoff (mm) of each event is calculated at a pixel scale by using the SCS Runoff Curve Number method (NRCS, 1972):

$$Q_{runoff} = \frac{(P - Ia)^2}{P - Ia + Sa} \quad (4)$$

$$Sa = \frac{25400}{CN} - 254 \quad (5)$$

$$Ia = 0.2 \times Sa \quad (6)$$

where P is the total precipitation of the event (mm); Sa is the storage parameter (mm); and Ia is the initial abstraction (mm). The Sa value spatially varies in respect to the soil characteristics and land use through the CN value.

Runoff generation analysis evaluates the influence of soil properties on water and sediment connectivity at a catchment scale, which permits considering significant spatial changes in these properties. The runoff also varies temporally, i.e., runoff generation can be different for each event. From the insertion of runoff in the assessment of water and sediment connectivity, it is possible to consider the spatial-temporal precipitation influence which is quite important for subtropical mountainous catchments. Where it should be noted that there is strong seasonality in precipitation.

Soil erosion results from detachment and transport of soil particles due to the raindrops impact and overland flow, among other processes. On interrill areas, raindrops impact causes mainly detachment but also transport according to slope steepness. In these areas, when runoff occurs it is responsible for sheet erosion, and the transport capacity of the runoff can be enhanced by the impact of the raindrops because it increases the turbulence level (Foster, 1982). On rills both sediment detachment and transport resulted from concentrated runoff, which depends on rainfall characteristics. Thus, rainfall amount and intensity control those processes and sediment availability.

The inclusion of Ips , proposed by Censi (2019), in the upstream component for the connectivity calculation brings a weighting in relation to the sediment amount that became available at the previous event to be connected during the analyzed event. The Ips has been designed considering some assumptions. The first one is that the soil particles detachment is related to the precipitation maximum intensity (Wischmeier and Smith, 1978; Morgan, 2005). According to Wischmeier and Smith (1978), precipitation erosivity consists of the precipitation potential to cause erosion, and it can be represented by the kinetic energy of the precipitation maximum intensity. The second assumption examines the total transported sediment that is related to the total runoff volume (Williams, 1978; Morgan, 2005), which is directly associated to

total precipitation. Williams (1978) assumed that, the sediment concentration also varies directly and linearly with runoff volume at the Instantaneous Unit Sediment Graph (IUSG).

The index was structured to express the availability of sediments given the characteristics of antecedent precipitation events, which refer to every precipitation event occurred before the current event. Sediment availability from determined antecedent event is supposed to be directly proportional to the precipitation intensity of such event. It is considered inversely proportional to the total precipitation of all the antecedent events between the current and the antecedent one in analysis. Thus, the greater the intensity of the antecedent precipitation event is, the greater it is the amount of detached sediment. The greater the total precipitation between such event and the current one is, the smaller it is the amount of sediment available for transport in the current event. The Ips can be calculated for any specified antecedent precipitation event:

$$Ips(j) = \frac{Imax_{m-j}}{\sum_{i=1}^j \frac{V_{m-i}}{\Delta t_{m-i}}} \quad (7)$$

where m means the current precipitation event; j represents the number of precipitation events between the current one and the antecedent one for which the Ips value is calculated; $Imax_{m-j}$ is the maximum intensity of the antecedent precipitation event $m-j$ (mm.d⁻¹); V_{m-i} is the accumulated precipitation of the antecedent event $m-i$ (mm); and Δt_{m-i} is the duration of the precipitation event $m-i$ (d). It is noted that the present study used the Ips calculated for the first antecedent event, i.e., $j = 1$.

The purpose of Ips formulation is not to quantitatively estimate the total sediment available for a certain rainfall event. Instead, it intends to establish a weighting aspect to represent the availability of sediment regarding antecedent conditions on the catchment. Thus, the Ips use permits considering the antecedent conditions of the catchment and comparing distinct precipitation events.

The IHC maintains a first order application, considering three new information, i.e., precipitation, land use and soil characteristics. An important limitation of the index is its incapability to deal with sediment exhaustion in the catchment when the sediment input in the system is source limited. This way, it can be said that IHC indicates, pixel by pixel, the potential to connectivity without considering the availability of sediment to be transported.

In applying the IHC for specific events, values and maps that reflect dynamic processes of the catchment are generated, besides concerning the functional and structural components of connectivity. The IHC was calculated at the catchment scale, with its outlet located at the Gauge Station 3 of the Mascarada River catchment (Fig. 1).

2.4. Data acquisition

The used Digital Terrain Model (DTM) has a spatial resolution of 1x1 m of cell size (grid). DTM has a vertical and horizontal accuracy of 2 m RMSE/3m LE90 (absolute) and 1 m RMSE/1.5 m LE90 (relative). This DTM is the AW3D Enhanced acquired from NTT DATA Corporation® generated from the combination of several high-resolution satellite images obtained with the Digital Globe satellite constellation. The vegetation recognized from the satellite images was removed from DSM (Digital Surface Model) through height estimations based on elevation differences observed in the borders between vegetated and unvegetated areas.

The used W values were those of RS obtained from land use maps. The defined RS values were the same presented in Zanandrea et al. (2020) which evaluated the influence of the use of different W in the calculation of IC for the Mascarada River catchment. According to the authors, the use of RS presented a better application for the same study area than other formulations used for W .

The precipitation data were obtained from 3 precipitation-stations located at different points within the study area (Fig. 1 and Table 1). The Mascarada River catchment also has water level and turbidity

Table 1
Description of Mascarada catchment monitoring system.

Station	Start	Parameter	Time interval
1*	18/12/2018	Precipitation	5 min
2*	01/08/2019	Precipitation	10 min
3*	04/02/2018	Precipitation, water level, turbidity	10 min
5**	11/25/2014	Precipitation	1 h

* Stations referring to Fig. 1.

** Station 5 is located outside the limits of the Mascarada River catchment, in Riozinho municipality.

monitoring at Station 3, located at the catchment outlet, and it has a series of discharge and sediment concentration, obtained through a rating curve.

Seven events were used in this study. To define the individual events, the significant precipitation value and the interval between precipitation events were used as criteria. Only events whose maximum precipitation was equal to or greater than 0.5 mm were considered, while the interval between precipitation events was established at 20 h, which indicates the response period of the catchment after the end of the precipitation event. For each event, the total precipitation was determined, and their corresponding I_{ps} value was calculated (Table 2). In order to simulate the event occurred in January 2017 (Event 7), the data measured by an unofficial rain gauge (Fig. 1) was used, because the automatic stations had not been installed yet inside the study catchment. For the calculation of I_{ps} and for the total precipitation (P) in the lower part of the catchment, the data from an automatic station outside the limits of the Mascarada River catchment, in the Riozinho municipality, located near the catchment outlet, were used for the Event 5.

Both P and I_{ps} values were spatially distributed in the catchment by the Thiessen Polygons method, assigning the values of P and I_{ps} for each pixel according to the designed polygon (Fig. 1). The CN values were also defined for each pixel (Fig. 1) based on the land-use map presented by Zanandrea et al. (2020), obtained by satellite images analysis and validated through field survey, and the soil map of the region (Düming et al., 2008). The catchment soil characteristics were confirmed by means of field tests (hydraulic conductivity and shear stress) and soil samples and laboratory analysis (granulometry). Those informations were used to classify the catchment soils according to the hydrologic soil group established by the NRCS (1970). After defining the spatialized CN values inside the catchment, a verification of the water budget was

Table 2
Precipitation event data (I_{ps} and P) for each gauge station.

Event	Date	Station	I_{ps}	P (mm)
1	05/27/2019 a 05/28/2019	1	39.20	31.80
		2	27.89	36.60
		3	18.36	38.80
2	06/30/2019 a 07/01/2019	1	16.94	32.40
		2	12.65	30.60
		3	2.37	37.20
3	07/30/2019 a 07/31/2019	1	49.40	14.20
		2	48.85	15.00
		3	23.08	14.20
4	09/17/2019 – 09/20/2019	1	60.43	63.80
		2	10.73	62.00
		3	13.00	45.00
5	10/17/2019 a 10/20/2019	1	30.49	61.20
		2	26.23	94.40
		3	27.28	57.20
6	11/04/2019 a 11/05/2019	1	98.60	63.80
		2	54.46	62.80
		3	41.00	56.20
7	01/05/2017	4*	3.00	272.00
		5	3.00	66.00

Rain gauge stations accuracy: $\pm 1\%$ (for $\leq 60 \text{ mm/h}$)/ $\pm 2\%$ (for 60 to 200 mm/h) and resolution: 0.2 mm.

* Station 4 is nonofficial gauge station (Fig. 1).

carried out based on the precipitation and discharge data collected in the catchment, in order to ensure the adequate representation of the defined CN values for the study area. In the calculation of the water budgets for some simulated events, an average error of 10% was found.

From these data the CN values were defined according to NRCS (1972), and only hydrological group of the soil was considered. Thus, the runoff of each cell was calculated for each event generating a spatialized Q_{runoff} map for the study catchment. We set the minimum Q_{runoff} value to 0.0001 mm to avoid computational errors. The values of the total runoff volume of the catchment were compared with the flow data measured at the catchment outlet in order to verify the representation of the model in the study area.

2.5. Temporal variability analysis and field data testing

The validation of connectivity maps is considered a challenge in the scientific community, because it is not yet possible to quantitatively identify the processes involved in the connectivity concept (Wohl, 2017; Heckmann et al., 2018; Zingaro et al., 2019). Several studies (e.g., Borselli et al., 2008; Cavalli et al., 2013; Wohl, 2017; Zingaro et al., 2019) used field data on sediment transfer processes and pathways, often related to extreme events such as landslides to validate connectivity indices. Thus, field surveys were conducted not only to investigate *in situ* the sites that presented higher and lower IHC values for the index validation, but also to identify sediment deposition and transfer sites within the catchment.

For comparison and verification of the Event 7 IHC , it was used an inventory of landslides scars and debris flows pathways, occurred due to the same precipitation event. Such inventory was obtained by aerial images interpretation and field research (Zanandrea et al., 2019). This detailed inventory clearly shows that most of the identified landslides are connected to the channels. It is well known that the sediments produced in this event reached the catchment outlet causing a flood with a high concentration of sediments and debris in the downstream municipality. Zingaro et al. (2019) portrayed that, given the complexity of processes related to sediment connectivity, the identification of sediment source and deposition areas can be used in the validation of connectivity indices. In addition, the IC was developed to assess the sediment pathways created by debris flows (Cavalli et al., 2013). Thus, considering that the IHC was based on IC , the evaluation of Event 7 by the scar inventory is appropriate. Finally, a quantitative analysis was also performed, by using the values of the peak flow and total runoff volume for other events measured at the catchment outlet for comparison with the mean and maximum IHC values (IHC_{mean} e IHC_{max}). The comparison between the measured and calculated values was also carried out with Pearson correlations (Pearson, 1896). The analyses were performed with Statistica © 13.0 and the p value of 0.01 was established to consider the statistically significant correlations for the other six events.

3. Results

3.1. Spatial-temporal variation in water and sediment connectivity

The IHC maps of the seven precipitation-events were generated with Eq. (3) at a catchment scale. Fig. 2 demonstrates results of five events in ascending order of magnitude of the mean precipitation. In Event 3, which has the lowest mean precipitation, there was the least connectivity of water and sediments with the Mascarada catchment outlet (Fig. 2). On other hand, there was an increase in IHC values with the increase in P and I_{ps} (Table 3), which depends spatially on the area affected by precipitation. It is observed that regions covered by forests located in the lower portion of the catchment close to the main river presented higher IHC values (Fig. 2) only when affected by events of larger magnitudes ($P > 50 \text{ mm}$) and with the higher I_{ps} .

In events of lower total precipitate and I_{ps} , regions located in the

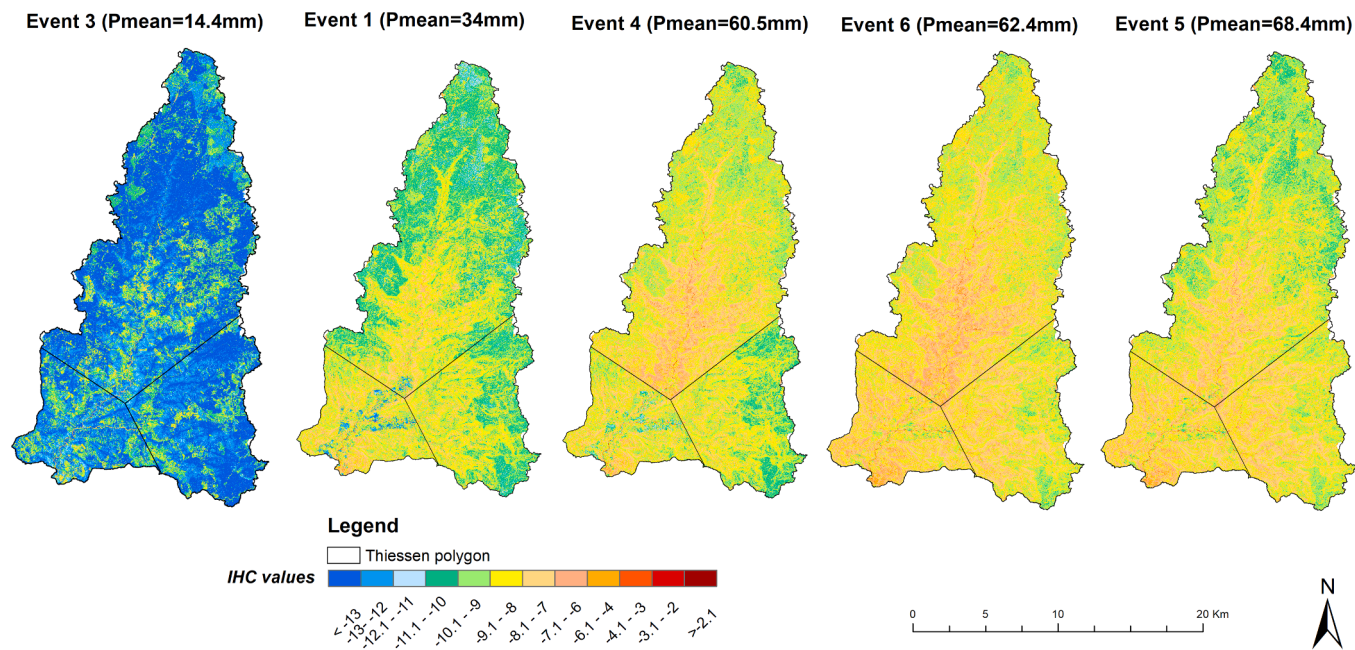


Fig. 2. IHC map for precipitation events in ascending magnitude order.

Table 3
Descriptive statistics of IHC events.

Event	P_{mean} (mm)	Ips_{mean}	IHC				
			Mean	Min.	Max.	Std.	Cv (%)
1	34.0	33.3	-9.10	-15.85	5.62	1.23	13.5
2	32.7	13.7	-9.61	-17.23	4.68	1.23	12.8
3	14.4	45.2	-12.41	-16.72	4.37	2.07	16.7
4	60.5	41.4	-8.40	-13.70	6.09	1.12	13.3
5	68.4	29.0	-8.33	-12.57	6.53	1.12	13.4
6	62.4	79.3	-7.98	-12.21	6.62	1.09	13.7
7	240	3	-8.5	-12.69	6.46	1.05	12.3

Std. = standard deviation Cv = coefficient of variation

floodplain, presented lower IHC values as highlighted in Fig. 3. These regions function as a sediment deposition area over most of the time, connecting to the outlet only in extreme events, which was observed by Joyce et al. (2018) too.

The statistics for all events are shown in Table 3. The lowest mean IHC was obtained for Event 3 which has the lowest mean precipitation, however, the minimum IHC value was obtained for Event 2 with the lowest average Ips . It occurred because the region of Station 3 (smaller area of influence) in Event 2 had the lowest Ips value, causing a lower value of the minimum IHC. Even being a small region, it did not significantly influence over the catchment. The values of standard deviation and coefficient of variation were similar among all events, except Event 3 that presented more variation.

According to Hu et al. (2019) and Tuset et al. (2016), there is a strong positive correlation between the magnitude of hydrological events and sediment yield. Therefore, the mean and maximum IHC values were compared with the peak flow and the total runoff volume of each event to verify the performance of the IHC (Fig. 4).

An increase of the IHC values is observed when there is an increase of

the total runoff volume and the peak flow. Only Event 1 showed a different behavior, although this event had a higher peak flow than Event 4, it had a lower runoff volume (Fig. 4). It took place because Event 4 was caused by less intense precipitation, i.e., with longer duration, which caused an event with two peak flows and consequently could increase sediment yield (Fig. 5).

According to Tuset et al. (2016), the sediment load is highly dependent on direct runoff. The IHC values were statistically correlated with the magnitude of the events (peak flow and total runoff volume) (Fig. 4). The correlation was high among the maximum IHC values, the total runoff volume (0.88) and the peak flow (0.83). The correlation was also positive, but it was relatively lower among the IHC_{mean} values, the total volume (0.69) and the peak flow (0.63). These values are close to those found by Tuset et al. (2016) when analyzing Pearson's correlation as to the measured values of total sediment load, the peak flow (0.79) and the runoff volume (0.67). Hu et al. (2019) found out similar results, too, by analyzing the linear correlation between the peak flow and the sediment yield (0.86).

3.2. IHC verification with field evidence

During the field surveys, the locations that showed the largest differences between the events in the IHC values were checked (Fig. 6). Though three flow paths were observed along a hillslope of native dense forest, only one of these paths, i.e., the point 11 in Fig. 6, had surface flow with the visual presence of suspended sediments being transported. The other points, i.e., 10 and 12 in Fig. 6, presented only the flow path on the ground and the deposition of coarse sediments in the path.

According to Hopp and McDonnell (2009), steep hillslopes intensify the hydrological response due to the increase in the elevation gradient and the slope angle. For Event 3, in which less runoff occurred the IHC value for point 11 (-7.2) was higher than points 10 and 12 (-8.3) with less connectivity to the outlet. In Event 6 with the highest runoff volume, all the three points had the same IHC value (-5.7), higher than in Event 3,

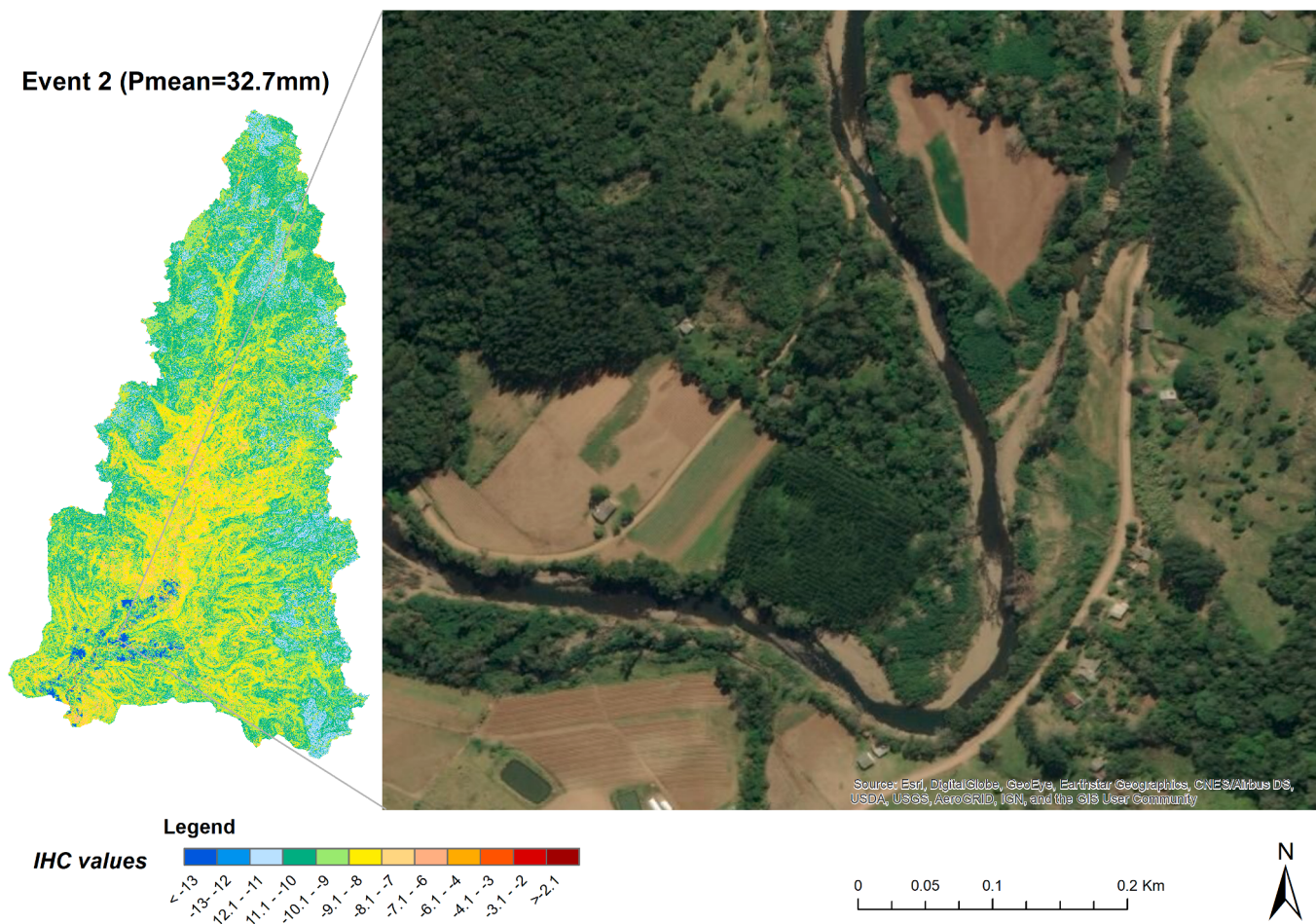


Fig. 3. Regions with sediment deposition in the floodplain disconnected to the outlet in low magnitude events.

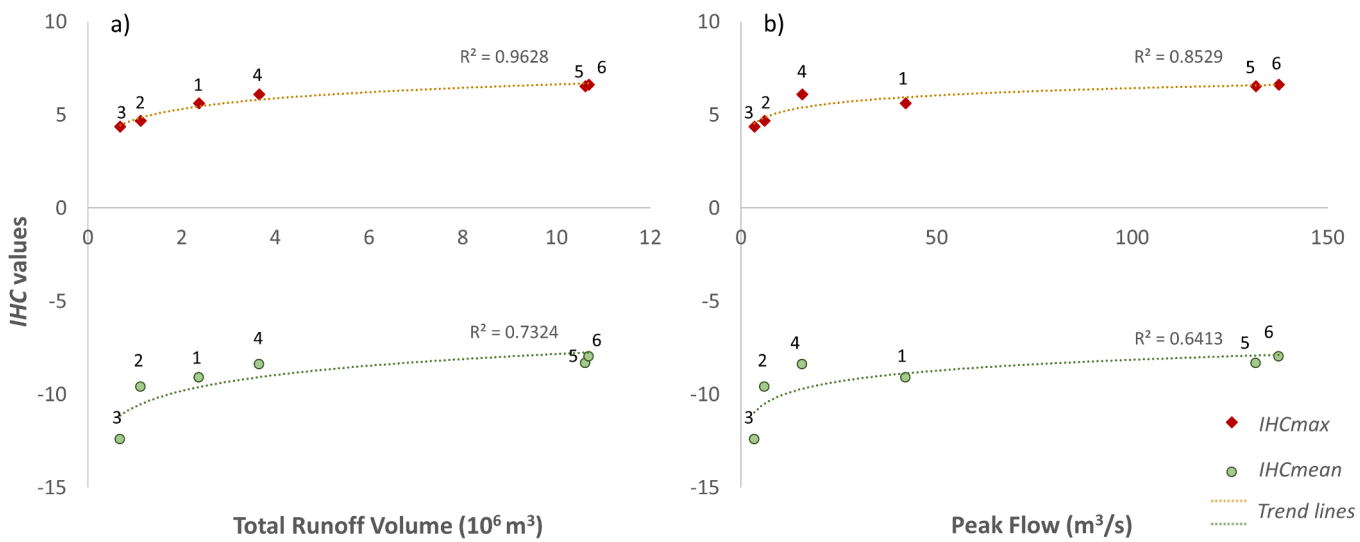


Fig. 4. Values of a) Mean IHC and maximum IHC and total runoff volume and b) Mean IHC and maximum IHC and peak flow for each event.

which indicates that in precipitation events of greater magnitude there is a significant contribution from the three presented flow paths. In the same way, it implies the connectivity dependence on the hillslope in the face of the regional pluviometry characteristics, causing an increase in the connectivity of the hillslope to the outlet.

3.3. IHC 2017 event

The IHC calculation was also carried out for the event that occurred in January 2017 (Event 7) which had a total mean precipitation of 240 mm, but this precipitation occurred only in the upper and middle parts of the Mascarada catchment (approximately 60% of the catchment

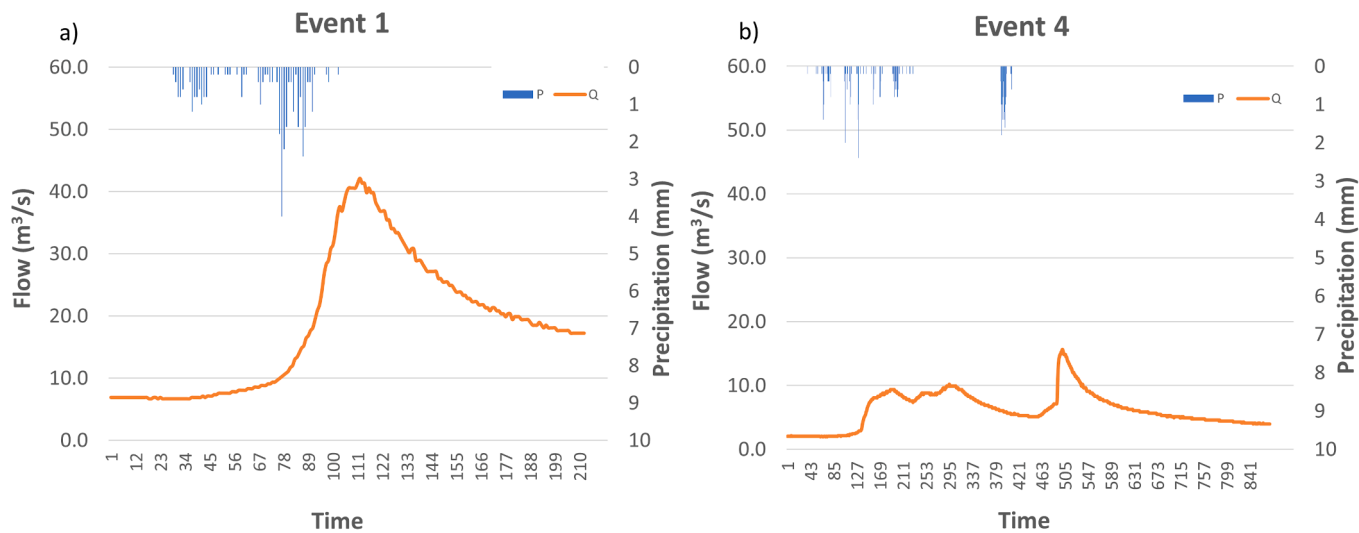


Fig. 5. Flow (Q) and precipitation (P) series: a) Event 1 and b) Event 4.

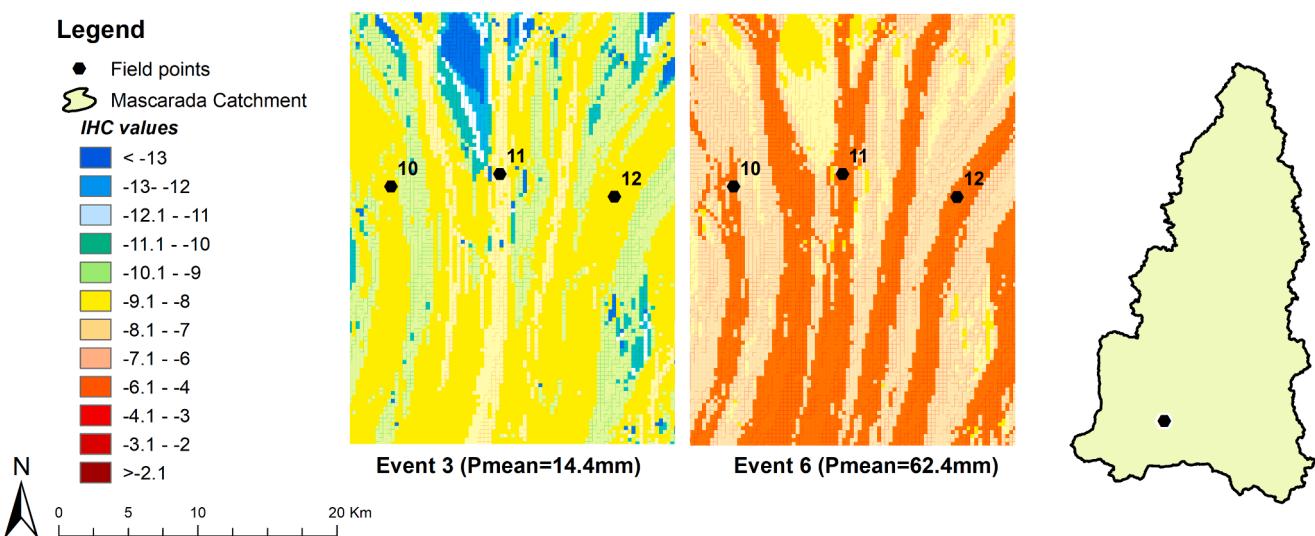


Fig. 6. IHC of the flow paths in hillslopes of the Mascarada Catchment.

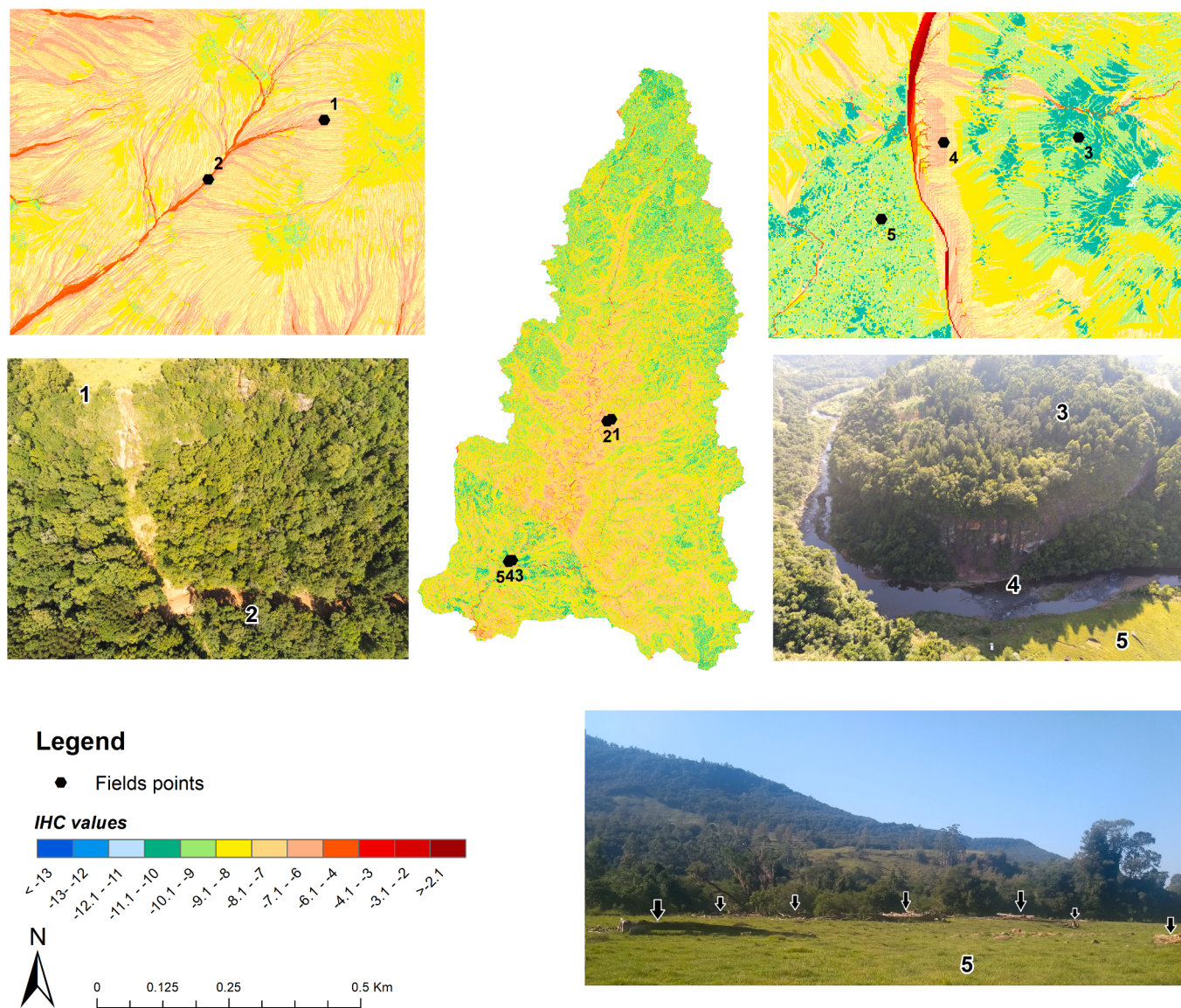


Fig. 7. IHC map of Event 7 ($P_{\text{mean}} = 240 \text{ mm}$) where several landslides and debris flows occurred in 2017.

area). The mean value of *IHC* was -8.5 . This value is lower than that of the other events with a lower total precipitate, mainly due to low *Ips*, i.e., little antecedent rain, causing less sediment available to be transported superficially. However, this event yielded a lot of sediments due to landslides and debris flow, that were well identified by the *IHC* (Fig. 7).

The verification of the landslides and debris flow occurrences was performed qualitatively through visual interpretation. In the middle region of the catchment (points 1 and 2 in Fig. 7) large debris flows were observed along the hillslope that reached the main channel, showing high *IHC* values in these places (*IHC* between -4.2 and -5.2). The presence of sediment deposits along the channel shows the connection of debris flows from the upper portion of the catchment to the lower regions, providing a supply of sediments to be transported into the channel (point 4 in Fig. 7). Furthermore, in some areas that showed lower connectivity values (*IHC* between -10.5 and -9.5), a kind of evidence was found in the field, such as woody debris and coarse sediments (point 5 in Fig. 7). These regions functioned as deposit areas during Event 7, disconnecting the catchment outlet from the upstream area.

4. Discussion

According to Najafi et al. (2021) a greater understanding of structural and functional sediment connectivity is expected to be able to explain how sediment dynamic occurs. This advance should decrease uncertainties in representing sediment processes at a catchment scale. However, once connectivity shows its own uncertainties, they can propagate through the calculations and potentially affect the results. The present study emphasizes that the uncertainties in the DTM generation may not represent the microtopography with accuracy mainly in forested areas, which may have been smoothed by the technique used to remove the vegetation from DSM. This can cause an increase in the connectivity of some areas (Heckmann et al., 2018), however, it does not become a deterrent, considering the low relevance of small-scale details in a catchment scale assessment.

Another source of uncertainty concerns the precipitation data. The measured values have a high accuracy considering the intensity of the events. Thus, the main precipitation uncertainty is associated to the spatial distribution. According to Batista et al., (2019), uncertainty in spatially explicit input data is high and data are difficult to obtain.

Nonetheless, several studies have shown that simple methodologies such as Thiessen's are capable of generating accurate results in catchment scale, especially when the rain gauges are well located (Cho et al. 2009; Gourbesville and Caignaert, 2020).

In terms of precipitation spatial-variability, the northeastern part of the catchment receives precipitation of larger magnitude, which favors the sediment mobilization in the mountainous area on steep hillslopes (Michaelides and Wainwright, 2002). Mountainous catchments have a strong influence on the precipitation spatial distribution, in addition to favoring erosive processes (Wohl, 2010). This can be seen in Event 4 (Fig. 2), where high-intensity precipitation, preceding the event, occurred in a concentrated way in the upper and middle region of the catchment and caused a high value of I_{ps} in this region. Thus, higher IHC values for this event occurred in the upper part of the catchment due to the greater availability of sediments to be connected to the outlet. When these mentioned values are compared to the southeastern portion, one can say it was not affected by this expressive antecedent precipitation.

The connectivity values are a function of the topographic features and land use, substantially researched so far. However, the hydrological forcing is also important and should be considered in the mobilization of sediments (Mishra et al., 2019). This causes connectivity to vary over a short time scale due to precipitation events, as observed in the regions close to the main river in the lower portion of the catchment. Gay et al. (2016), by their turn, reported that topographic indexes do not reflect the real connectivity of sediments in lowland areas, and the insertion of hydrological aspects such as the persistence of the drainage network can improve this representation. On the other hand, the connectivity of these areas is so dynamic that the approach used through runoff events has advantages in terms of the temporal water variability and sediment connectivity as well.

In addition to the characteristics of precipitation events (Puigdefá-bregas, 2005; Turnbull and Wainwright, 2019), the sediment connectivity of a catchment is controlled by the relief forms together with the spatial arrangement of the hydrogeomorphic processes that control the water and sediment transfer rates (Slaymaker, 2006; Heckmann et al., 2018). The connectivity between landscape compartments, such as hillslope and channel, and the one with the catchment outlet is a dynamic process. Turnbull et al. (2008) mentioned that the heterogeneity of connectivity patterns, even when present in small proportions, affects the hydrological response and causes changes in the general behavior of a system. As seen in Fig. 6, variations in the connectivity of the paths from event to event reflect changes in the coupling state of the system, i.e., temporal variations in connectivity. According to Heckmann et al. (2018), these variations cause changes in the morphodynamics and sediment yield of the catchment. The IHC map presented agreement with the field observations and it represented the sediment (dis)connectivity patterns, such as sediment transport paths and area of debris deposits in the catchment, mainly during the event of January 2017 (Event 7). The landslides scars and debris flow paths, represented by exposed soil, located on steep hillslopes, are considered hotspots, generating rapid runoff which triggers erosion (Marchamalo et al., 2016; Mishra et al., 2019). These hotspots have a dynamic contribution to the sediment yield of the catchment, once they are activated only in some events of higher magnitude, affecting the temporal variation of sediment connectivity.

5. Conclusion

A modification of the connectivity index (IC) by Borselli et al. (2008) was proposed based on the inclusion of precipitation and runoff characteristics at an event scale. This approach, called Hydro-sedimentological Connectivity Index (IHC), combines functional and structural properties to assess the water and sediment connectivity. The insertion of functional components (surface runoff and antecedent precipitation index) permitted obtaining a temporal variation of connectivity in the catchment, previously only spatially varied.

The IHC allows assessing the variation in connectivity over time under different precipitation events, spatialized according to the area affected by the precipitation. The generation of spatially-distributed runoff allows assessing the locations and precipitation events in which a given region could be most connected to the outlet. The parameter I_{ps} included the idea of sediment availability, indicating whether in a specific event there is more or less sediment available to be connected when compared to other events. The IHC map identified areas of sediment transfer and deposition consistent with field observation, and it also showed consistency with the extreme event that occurred in the catchment, identifying landslides, debris flow and deposition areas. A quantitative verification of the IHC can be confirmed with a high correlation of IHC with the total runoff volume and the peak flow, which are both measured in the catchment outlet.

The IHC was an attempt to estimate the spatial-temporal variation of water and sediment connectivity in a catchment and to identify locations of sediment transfer and deposition for precipitation events of different magnitudes. The main advances of the IHC use are: (i) to bring the possibility of comparing connectivity patterns created by different precipitation events in the same catchment; (ii) to consider the spatial distribution of precipitation within the catchment; and (iii) to allow comparison of connectivity patterns between catchments under different hydrological regimes. When directly comparing IHC values between different catchments it is important to keep the same spatial resolution, because Q_{runoff} depends on the pixel size. These advances permit representing, at least initially, the spatial-temporal variability of connectivity through functional components.

Though the IHC can bring advances to connectivity representation, it has some limitations. The main limitations of the method are: (i) the use of tabulated values (e.g., n and CN), whose choice depends highly on the user's level of knowledge about the study area, showing subjectivity to the assessment; (ii) the IHC does not represent the physical interaction between the structural and functional components; and (iii) I_{ps} is not able to quantify the actual quantity of available sediment. Hence, it is only able to indicate a probability of a larger amount of sediment to be available when compared to other events. Thus, the index is not able to represent sediment exhaustion in the catchment.

Regarding the first limitation, the choice of the tabulated parameters must be performed based on available catchment data. If possible, it is really recommended to carry out field survey and to use observation data in order to reduce uncertainties. If the input parameters are well defined, the IHC can indicate important places of higher and lower connectivity and precipitation thresholds for the occurrence of (des) connectivity of some areas, which can be useful for catchment management.

Declaration of Competing Interest

The authors declare that they have no known competing financial interests or personal relationships that could have appeared to influence the work reported in this paper.

Acknowledgements

This study was financed in part by Coordenação de Aperfeiçoamento de Pessoal de Nível Superior - Brasil (CAPES). It was also supported by the CNPQ (grant numbers 428175/2016-3) and CAPES-ANA projects (grant numbers 16/2017, Finance Code 001). And finally we would like to acknowledge Mágat Nágelo Junges for the English review

References

- Baartman, J.E.M., Nunes, J.P., Masselink, R., Darboux, F., Bielders, C., Degre, A., Cantreul, V., Cerdan, O., Grangeon, T., Fiener, P., Wilken, F., Schindewolf, M., Wainwright, J., 2020. What do models tell us about water and sediment connectivity?, 107300 Geomorphol. GEOMOR. <https://doi.org/10.1016/j.geomorph.2020.107300>.

- Batista, P.V.G., Davies, J., Silva, M.L.N., Quinton, J.N., 2019. On the evaluation of soil erosion models: are we doing enough? *Earth-Sci. Rev.* 197 (2019) <https://doi.org/10.1016/j.earscirev.2019.102898>.
- Borselli, L., Cassi, P., Torri, D., 2008. Prolegomena to sediment and flow connectivity in the landscape: a GIS and field numerical assessment. *Catena* 75, 268–277. <https://doi.org/10.1016/j.catena.2008.07.006>.
- Bracken, L., Turbull, L., Wainwright, J., Bogaart, P., 2015. Sediment connectivity: a framework for understanding sediment transport at multiple scales. *Earth Surf. Process. Landf.* 40 (2), 177–188. <https://doi.org/10.1002/esp.3635>.
- Bracken, L.J., Wainwright, J., Ali, G.A., Tetzlaff, D., Smith, M.W., Reaney, S.M., Roy, A. G., 2013. Concepts of hydrological connectivity: research approaches, pathways and future agendas. *Earth Sci. Rev.* 119, 17–34. <https://doi.org/10.1016/j.earscirev.2013.02.001>.
- Cavalli, M., Trevisani, S., Comiti, F., Marchi, L., 2013. Geomorphometric assessment of spatial sediment connectivity in small Alpine catchments. *Geomorphology* 188, 31–41. <https://doi.org/10.1016/j.geomorph.2012.05.007>.
- Censi, G., 2019. Tank model modificado para escoamento e produção de sedimentos. Masters thesis. UFRGS, Porto Alegre, 208f.
- Chartin, C., Evrard, O., Laceby, J.P., Onda, Y., Ottlé, C., Lefèvre, I., Cerdan, O., 2017. The impact of typhoons on sediment connectivity: lessons learnt from contaminated coastal catchments of the Fukushima Prefecture (Japan). *Earth Surf. Process. Landf.* 42, 306–317. <https://doi.org/10.1002/esp.4056>.
- Cho, J., Bosch, D., Lowrance, R., Strickland, T., Velliidis, G., 2009. Effect of spatial distribution of rainfall on temporal and spatial uncertainty of SWAT output. *Trans. ASABE* 52 (5), 1545–1556. <https://doi.org/10.13031/2013.29143>.
- Chow, V.T., 1959. *Open-Channel Hydraulics*. McGraw-Hill, New York.
- Crema, S., Cavalli, M., 2018. SedInConnect: a stand-alone, free and open source tool for the assessment of sediment connectivity. *Comput. Geosci.* 111, 39–45. <https://doi.org/10.1016/j.cageo.2017.10.009>.
- de Walque, B., Degré, A., Maugnard, A., Bielders, C.L., 2017. Artificial surfaces characteristics and sediment connectivity explain muddy flood hazard in Wallonia. *Catena* 158, 89–101. <https://doi.org/10.1016/j.catena.2017.06.016>.
- Di Stefano, C., Ferro, V., 2018. Modelling sediment delivery using connectivity components at the experimental SPA2 basin, Sicily (Italy). *J. Mt. Sci.* 15 (9), 1868–1880. <https://doi.org/10.1007/s11629-018-4956-8>.
- Düning, A., Schad, P., Kohok, M., Beyerlein, P., Schwimmer, W., Kögel-Knabner, I., 2008. A mosaic of nonallopathic Andosols, Umbrisols and Cambisols on rhyodacite in the southern Brazilian highlands. *Geoderma* 145, 158–173. <https://doi.org/10.1016/j.geoderma.2008.01.013>.
- Duvert, C., Gratiot, N., Anguiano-Valencia, R., Némery, J., Mendoza, M.E., Carlón-Allende, T., Prat, C., Esteves, M., 2011. Baseflow control on sediment flux connectivity: Insights from a nested catchment study in Central Mexico. *Catena* 87 (1), 129–140. <https://doi.org/10.1016/j.catena.2011.05.021>.
- Foster, G.R., 1982. Modeling the erosion process. In: Haan, C.T., Johnson, H.P., Brakensiek, D.L. (Eds.), *Hydrologic Modeling of Small Watersheds*. St. Joseph: American Society of Agricultural Engineering, pp. 297–380.
- Gay, A., Cerdan, O., Mardhel, V., Desmet, M., 2016. Application of an index of sediment connectivity in a lowland area. *J. Soils Sediments* 16 (1), 280–293. <https://doi.org/10.1007/s11368-015-1235-y>.
- Gourbesville, P., Caignaert, G., 2020. Advances in Hydroinformatics (SimHydro 2019 - Models for Extreme Situations and Crisis Management), Springer Water, 1077p. doi: 10.1007/978-981-15-5436-0.
- Heckmann, T., Cavalli, M., Cerdan, O., Foerster, S., Javaux, M., Lode, E., Smetanová, A., Vericat, D., Brardinoni, F., 2018. Indices of sediment connectivity: opportunities, challenges and limitations. *Earth Sci. Rev.* 187, 77–108. <https://doi.org/10.1016/j.earscirev.2018.08.004>.
- Hicks, D.M., Gomez, B., Trustrum, N.A., 2000. Erosion thresholds and suspended sediment yields, Waipaoa River Basin, New Zealand. *Water Resour. Res.* 36 (4), 1129–1142. <https://doi.org/10.1029/1999WR900340>.
- Hopp, L., McDonnell, J.J., 2009. Connectivity at the hillslope scale: Identifying interactions between storm size, bedrock permeability, slope angle and soil depth. *J. Hydrol.* 376 (3–4), 378–391. <https://doi.org/10.1016/j.jhydrol.2009.07.047>.
- Hu, J., Gao, P., Mu, X., Zhao, G., Sun, W., Li, P., Zhanh, L., 2019. Runoff-sediment dynamics under different flood patterns in a Loess Plateau catchment, China. *Catena* 173, 234–245. <https://doi.org/10.1016/j.catena.2018.10.023>.
- Jones, K.E., Preston, N.J., 2012. Spatial and temporal patterns of off-slope sediment delivery for small catchments subject to shallow landslides within the Waipaoa catchment, New Zealand. *Geomorphology* 141–142, 150–159. <https://doi.org/10.1016/j.geomorph.2011.12.037>.
- Joyce, H.M., Hardy, R.J., Warburton, J., Large, A.R.G., 2018. Sediment continuity through the upland sediment cascade: geomorphic response of an upland river to an extreme flood event. *Geomorphology* 317, 45–61. <https://doi.org/10.1016/j.geomorph.2018.05.002>.
- Kalantari, Z., Cavalli, M., Cantone, C., Crema, S., Destouni, G., 2017. Flood probability quantification for road infrastructure: Data-driven spatial-statistical approach and case study applications. *Sci. Total Environ.* 581–582, 386–398. <https://doi.org/10.1016/j.scitotenv.2016.12.147>.
- Kalantari, Z., Ferreira, C.S.S., Koutsouris, A.J., Ahlmer, A., Cerdà, A., Destouni, G., 2019. Assessing flood probability for transportation infrastructure based on catchment characteristics, sediment connectivity and remotely sensed soil moisture. *Sci. Total Environ.* 661, 393–406. <https://doi.org/10.1016/j.scitotenv.2019.01.009>.
- Korup, O., McSaveney, M.J., Davies, T.R., 2004. Sediment generation and delivery from large historic landslides in the Southern Alps, New Zealand. *Geomorphology* 61 (1–2), 189–207. <https://doi.org/10.1016/j.geomorph.2004.01.001>.
- Lane, S.N., Reaney, S.M., Heathwaite, A.L., 2009. Representation of landscape hydrological connectivity using a topographically driven surface flow index. *Water Resour. Res.* 45, W08423. <https://doi.org/10.1029/2008wr007336>.
- Leigh, E.G., 1975. Structure and climate in tropical rain forest. *Annu. Rev. Ecol. Syst.* 6, 67–86.
- López-Vicente, M., Ben-Salem, N., 2019. Computing structural and functional flow and sediment connectivity with a new aggregated index: a case study in a large Mediterranean catchment. *Sci. Total Environ.* 651, 179–191. <https://doi.org/10.1016/j.scitotenv.2018.09.170>.
- López-Vicente, M., Poesen, J., Navas, A., Gaspar, L., 2013. Predicting runoff and sediment connectivity and soil erosion by water for different land use scenarios in the Spanish Pre-Pyrenees. *Catena* 102, 62–73. <https://doi.org/10.1016/j.catena.2011.01.001>.
- Mahoney, D.T., Fox, J.F., Aamery, N.A., 2018. Watershed erosion modeling using the probability of sediment connectivity in a gently rolling system. *J. Hydrol.* 561, 862–883. <https://doi.org/10.1016/j.jhydrol.2018.04.034>.
- Marchamalo, M., Hooke, J.M., Sandercock, P.J., 2016. Flow and sediment connectivity in semi-arid landscapes in SE Spain: patterns and controls. *Land Degrad. Dev.* 27, 1032–1044. <https://doi.org/10.1002/ldr.2352>.
- Michaelides, K., Chappell, A., 2009. Connectivity as a concept for characterising hydrological behavior. *Hydrol. Process.* 23, 517–522. <https://doi.org/10.1002/hyp.7214>.
- Michaelides, K., Wainwright, J., 2002. Modelling the effects of hillslope-channel coupling on catchment hydrological response. *Earth Surf. Process. Landf.* 27, 1441–1457. <https://doi.org/10.1002/esp.440>.
- Mishra, K., Sinha, R., Jainb, V., Nepal, S., Uddin, K., 2019. Towards the assessment of sediment connectivity in a large Himalayan river basin. *Sci. Total Environ.* 661, 251–265. <https://doi.org/10.1016/j.scitotenv.2019.01.118>.
- Morgan, R.P.C., 2005. *Soil Erosion and Conservation*, third ed. Blackwell Publishing, Oxford.
- Najafi, S., Dragovich, D., Heckmann, T., Sadeghi, S.H., 2021. Sediment connectivity concepts and approaches. *Catena* 196. <https://doi.org/10.1016/j.catena.2020.104880>.
- Natural Resource Conservation Service NRCS, 1972. "Hydrology." National engineering handbook, Sec. 4, U.S. Department of Agriculture, Washington, D.C.
- Nunes, J.P., Wainwright, J., Bielders, C.L., Darboux, F., Fiener, P., Finger, D., Turnbull, L., Connecteur WG3 Think-Tank, 2018. Better models are more effectively connected models. *Earth Surf. Process. Landform.* 43 (6), 1355–1360. <https://doi.org/10.1002/esp.4323>.
- Pearson, K., 1896. Mathematical contributions to the theory of evolution. III. Regression, heredity, and panmixia. *Philos. Trans. R. Soc. Lond. Ser. A* 187, 253–318.
- Persichillo, M.G., Bordonali, M., Cavalli, M., Crema, S., Meisina, C., 2018. The role of human activities on sediment connectivity of shallow landslides. *Catena* 160, 261–274. <https://doi.org/10.1016/j.catena.2017.09.025>.
- Peters, D.P., Groffman, P.M., Nadelhoffer, K.J., Grimm, N.B., Collins, S.L., Michener, W. K., Huston, M.A., 2008. Living in an increasingly connected world: a framework for continental-scale environmental science. *Front. Ecol. Environ.* 6 (5), 229–237. <https://doi.org/10.1890/070098>.
- Puigdefàbregas, J., 2005. The role of vegetation patterns in structuring runoff and sediment fluxes in drylands. *Earth Surf. Process. Landform.* 30 (2), 133–147. <https://doi.org/10.1002/esp.1181>.
- Renard, K., Foster, G.R., Weessies, G.A., Mc Cool, D.K., Yodler, D.C., 1997. Predicting soil erosion by water—a guide to conservation planning with the Revised Universal Soil Loss Equation (RUSLE). U.S.D.A.-A.R.S., Agriculture Handbook, 703.
- SCS, 1972. Soil Conservation Service, U.S. Department of Agriculture, National Engineering Handbook. vol. 4. Hydrology: U.S. Government Printing Office, Washington, D.C.
- Slaymaker, O., 2006. Towards the identification of scaling relations in drainage basin sediment budgets. *Geomorphology* 80 (1–2), 8–19. <https://doi.org/10.1016/j.geomorph.2005.09.004>.
- Turnbull, L., Wainwright, J., Brazier, R.E., 2008. A conceptual framework for understanding semi-arid land degradation: ecohydrological interactions across multiple space and time scales. *Ecohydrology* 1 (1), 23–34. <https://doi.org/10.1002/eco.4>.
- Turnbull, L., Wainwright, J., 2019. From structure to function: understanding shrub encroachment in drylands using hydrological and sediment connectivity. *Ecol. Indic.* 98, 608–618. <https://doi.org/10.1016/j.ecolind.2018.11.039>.
- Tuset, J., Vericat, D., Batalla, R.J., 2016. Rainfall, runoff and sediment transport in a Mediterranean mountainous catchment. *Sci. Total Environ.* 540, 114–132. <https://doi.org/10.1016/j.scitotenv.2015.07.0750048-9697>.
- Wainwright, J., Turnbull, L., Ibrahim, T.G., Lexartza-Artza, I., Thornton, S.F., Brazier, R. E., 2011. Linking environmental régimes, space and time: Interpretations of structural and functional connectivity. *Geomorphology* 126 (3–4), 387–404. <https://doi.org/10.1016/j.geomorph.2010.07.027>.
- Ward, J.V., 1997. An expansive perspective of riverine landscapes: pattern and process across scales. *River Ecosys.* 6, 52–60. <https://doi.org/10.14512/gaia.6.1.6>.
- Williams, J.R., 1978. A sediment graph model based on an instantaneous unit sediment graph. *Water Resour. Res.* 14 (4), 659–664.
- Wischmeier, W.H., Smith, D.D., 1978. Predicting rainfall erosion losses — a guide to conservation planning. Agriculture Handbook, 537. U.S. Department of Agriculture.
- Wohl, E., 2010. Mountain Rivers Revisited. American Geophysical Union, Washington, p. 573 p. <https://doi.org/10.1029/WM019>.
- Wohl, E., 2017. Connectivity in rivers. *Prog. Phys. Geogr.* 41 (3), 345–362. <https://doi.org/10.1177/0309133117714972>.

- Wollmann, C.A., Galvani, E., 2012. Caracterização climática regional do Rio Grande do Sul: dos estudos estáticos ao entendimento da gênese. *Revista Brasileira de Climatologia*. 11, 87–103.
- Zanandrea, F., Michel, G.P., Kobiyama, M., Cardozo, G.L., 2019. Evaluation of different DTMs in sediment connectivity determination in the Mascarada River Watershed, southern Brazil. *Geomorphology* 332, 80–87. <https://doi.org/10.1016/j.geomorph.2019.02.005>.
- Zanandrea, F., Michel, G.P., Kobiyama, M., 2020. Impediment influence on the index of sediment connectivity in a forested mountainous catchment. *Geomorphology* 351. <https://doi.org/10.1016/j.geomorph.2019.106962>.
- Zhao, G., Gao, P., Tian, P., Sun, W., Hu, J., Mu, X., 2020. Assessing sediment connectivity and soil erosion by water in a representative catchment on the Loess Plateau, China. *Catena* 185. <https://doi.org/10.1016/j.catena.2019.104284>.
- Zingaro, M., Refice, A., Giachetta, E., D'Addabbo, A., Lovergine, F., De Pasquale, V., Pepe, G., Brandolini, P., Cevasco, A., Capolongo, D., 2019. Sediment mobility and connectivity in a catchment: A new mapping approach. *Sci. Total Environ.* 672, 763–775. <https://doi.org/10.1016/j.scitotenv.2019.03.461>.